

available at [www.sciencedirect.com](http://www.sciencedirect.com)[www.elsevier.com/locate/matchar](http://www.elsevier.com/locate/matchar)

# Investigation on hot deformation behavior of 00Cr23Ni4N duplex stainless steel under medium–high strain rates

Ying Han<sup>a,b</sup>, Dening Zou<sup>a,\*</sup>, Zhiyu Chen<sup>a</sup>, Guangwei Fan<sup>b,c</sup>, Wei Zhang<sup>c</sup>

<sup>a</sup>School of Metallurgy and Engineering, Xi'an University of Architecture and Technology, Xi'an, Shaanxi 710055, China

<sup>b</sup>State Key Laboratory for Mechanical Behavior of Materials, Xi'an Jiaotong University, Xi'an, Shaanxi 710049, China

<sup>c</sup>State Key Laboratory of Advanced Stainless Steel Materials, Taiyuan Iron and Steel (Group) Co., Ltd., Taiyuan, Shanxi 030003, China

## ARTICLE DATA

### Article history:

Received 11 October 2010

Received in revised form

24 November 2010

Accepted 29 November 2010

### Keywords:

Duplex stainless steel

Hot deformation

Medium–high strain rate

Zener–Hollomon parameter

Processing map

## ABSTRACT

The hot deformation behavior of 00Cr23Ni4N duplex stainless steel under medium–high strain rates ( $5\text{--}50\text{ s}^{-1}$ ) has been analyzed using the Zener–Hollomon parameter and processing maps, which is based on compression tests made at temperatures ranging from 900 to 1150 °C. The results display the significant influence of high strain rate and high temperature on hot deformation behavior of 00Cr23Ni4N duplex stainless steel. A classical hyperbolic sine equation is applied to reveal the relations between the peak stress, strain rate and deformation temperature, in which the activation energy,  $Q$  and stress exponent,  $n$  are 263.4 kJ/mol and 2.6, respectively. The Zener–Hollomon parameters at low and high temperatures are calculated respectively to reflect the microstructural evolutions. Based on the processing map obtained, an ideal hot working condition for commercial processing is in the temperature range between 1075 and 1150 °C with a strain rate of 10 to 30  $\text{s}^{-1}$ . Under such condition, both ferrite and austenite dynamic re-crystallizations can be obtained and the corresponding Zener–Hollomon parameter is relatively low. Furthermore, the unstable domains are indicated by the processing map.

© 2010 Elsevier Inc. All rights reserved.

## 1. Introduction

Due to the excellent combination of high strength and toughness, good weldability with superior resistance under critical working conditions, duplex stainless steel has been widely used in diverse fields, such as petroleum refining, paper manufacturing and ocean industries etc. [1–3]. Such good properties of duplex stainless steel rely on a two-phase microstructure comprised by approximately equal amounts of austenite and ferrite [4]. Therefore, the high performance and special microstructures have made duplex stainless steel a special class in all stainless steels.

Duplex stainless steel can be processed by different procedures, i.e. casting, forging, extrusion or rolling. These forming operations are usually performed at high temperatures where duplex stainless steel still has duplex structure and prefers

medium–high strain rates especially for commercial processing. However, different coefficients of thermal expansion and deformation behaviors of each constituent phase, austenite or ferrite, are considerably affected by the presence of the other phase under hot working conditions, which can lead to edge cracks or an inappropriate surface finish [5,6]. It is established that ferrite (body centered cubic), with rather high stacking fault energy, easily undergoes dynamic recovery to soften during hot deformation. On the other hand, austenite (face centered cubic), characterized by significantly lower stacking fault energy, undergoes only limited dynamic recovery and is likely to have dynamic re-crystallization [7–9]. Generally, the restoration process in ferrite for duplex stainless steel is found to be far in advance of that in austenite.

One method to investigate the hot deformation behavior of duplex stainless steel is to derive a constitutive relation for the

\* Corresponding author. Tel.: +86 29 82201074; fax: +86 29 82202923.  
E-mail address: [zoudening@sina.com](mailto:zoudening@sina.com) (D. Zou).

flow stress with processing variables under hot working conditions. It has been noticed that the peak stress or steady-state stress with different working parameters is of great importance in studying hot deformation behavior of alloys [10]. In this paper, the peak stress obtained from the flow curves will be considered. At high temperatures, the strain rate and deformation temperature-dependence of the peak stress can be described by the classical hyperbolic sine equation [7,9,10]:

$$Z = \dot{\epsilon} \exp(Q/RT) = A [\sinh(a \cdot \sigma_p)]^n \quad (1)$$

where  $Z$  is Zener–Hollomon ( $Z$ ) parameter,  $\dot{\epsilon}$  the strain rate ( $s^{-1}$ ),  $Q$  the activation energy for hot working (J/mol),  $R$  the universal gas constant,  $T$  the deformation temperature (K),  $A$  the material constant ( $s^{-1}$ ),  $\alpha$  the constant,  $\sigma_p$  the peak stress (MPa), and  $n$  the stress exponent. Accordingly, before describing the flow behavior of the steel with this equation,  $A$ ,  $\alpha$ ,  $n$  and  $Q$  need to be established first by experiments.  $Z$  parameter can be used to characterize the combined effect of temperature and strain rate on the deformation process, especially on the deformation resistance and microstructural evolutions. The lower the  $Z$  value is, the more effectively the dynamic recovery and dynamic re-crystallization occur, and the smaller deformation resistance value is during hot deformation. There will be a critical value  $Z_c$  for the  $Z$  parameter, over which dynamic re-crystallization hardly occurs in the alloy [11].

The processing map technique developed in recent years is another useful method to determine optimum processing parameters under hot deformation. It superimposes a power dissipation map and instability map, which is developed on the basis of the Dynamic Materials Model by Prasad et al. [12]. In this model, the work piece deformed under hot working conditions is considered to be a power dissipater. The power might be instantaneously dissipated into two complementary parts: the power dissipated by plastic work and the power dissipated by metallurgical processes. The efficiency of power dissipation ( $\eta$ ) occurring through microstructural changes during deformation is given by:

$$\eta = \frac{2m}{m+1} \quad (2)$$

in which  $m$  is the strain rate sensitivity of flow stress given by  $(\partial \log \sigma) / \partial (\log \dot{\epsilon})$ . The power dissipation map can be obtained on the basis of the values of  $\eta$  under different conditions.

The extremum principles of irreversible thermodynamics as applied to continuum mechanics of large plastic flow are employed to define a continuum criterion to obtain metallurgical instability during the plastic flow [12], as shown in Eq. (3):

$$\xi(\dot{\epsilon}) = \frac{\partial \ln[m / (m+1)]}{\partial \ln \dot{\epsilon}} + m \leq 0 \quad (3)$$

Flow instabilities are predicted to occur when  $\xi$  is negative, and then the instability map can be obtained. Therefore, the variation of parameters of  $\eta$ ,  $\xi$ ,  $\dot{\epsilon}$  and  $T$  constitutes the processing map directly. Each domain on the map can reflect microstructural mechanisms through the dissipation characteristics varied with different operating under those conditions of the domain. Nowadays, processing maps have been applied successfully in alloys of magnesium, aluminum,

**Table 1 – Chemical composition of 00Cr23Ni4N DSS (wt.%).**

C	Si	Mn	Cr	Ni	Mo	N	P	S	Fe
0.02	0.5	1.2	23.5	4.0	0.4	0.13	0.024	0.002	Bal.

titanium and Ni-based super alloys as well as stainless steels such as AISI 304L, 304, 316L and 22Cr–1Ni–0.7Mo duplex stainless steel [11,13–19].

Low-alloyed 00Cr23Ni4N duplex stainless steel, with good performance and a comparatively lower cost, can replace 304, 304L, 316 and 316L austenite stainless steels under certain conditions [20]. In this work, we will focus on the hot deformation mechanism of this steel under medium–high strain rates in the temperature range of 900–1150 °C, based on the  $Z$  parameter and processing maps.

## 2. Materials and Methods

The experimental material for this study is 00Cr23Ni4N duplex stainless steel, commercially produced by Taiyuan Iron and Steel (Group) Co. Ltd. Its chemical composition is listed in Table 1 and microstructure before hot deformation is shown in Fig. 1. It is clear that acicular austenite is distributed in the ferrite matrix as cast. Hot compression tests were conducted on a Gleeble-3800 thermo-mechanical simulator with cylindrical specimens of 10 mm in diameter and 15 mm in height over the range of temperatures from 900 to 1150 °C at 50 °C intervals and strain rates from 5 to 50  $s^{-1}$  at intervals of an order of magnitude. The specimens were experimented in the first heating up to 1230 °C for 4 min, and then cooling them to testing temperature at about 5 °C/s. All tests were performed to a total true strain of 0.9. The specimens were quenched immediately after hot compression in order to study the microstructural evolutions under high temperatures. Before

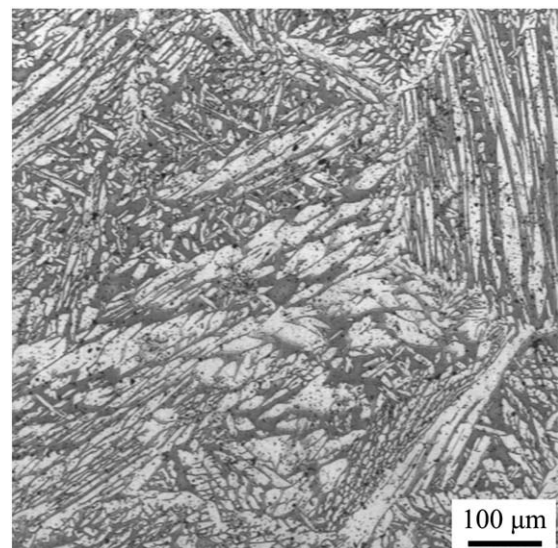


**Fig. 1 – The microstructure of 00Cr23Ni4N duplex stainless steel before hot deformation.**

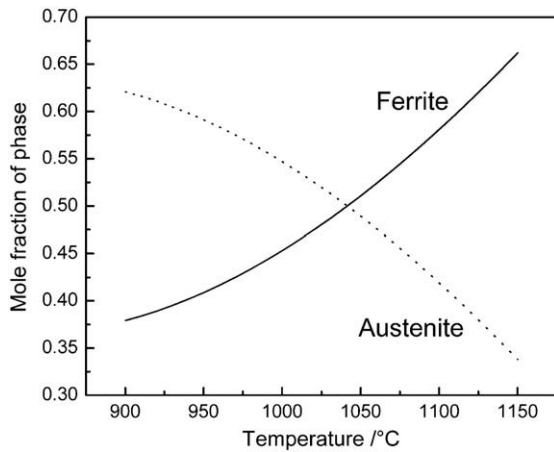


**Fig. 2** – The phase diagram calculated by using the Thermo-calc software for 00Cr23Ni4N duplex stainless steel.

observing microstructures along the longitudinal surface using optical microscopy, the specimens were electrolytic etched in oxalic acid solution.

### 3. Results and Discussion

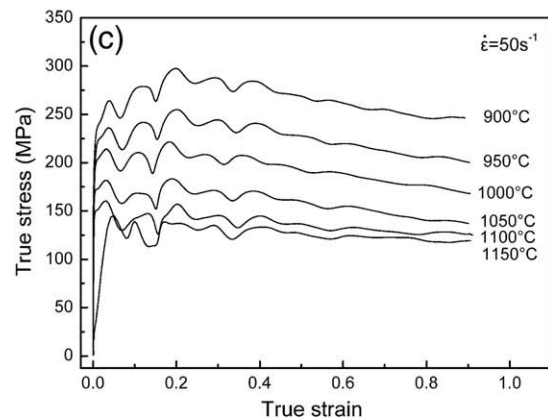
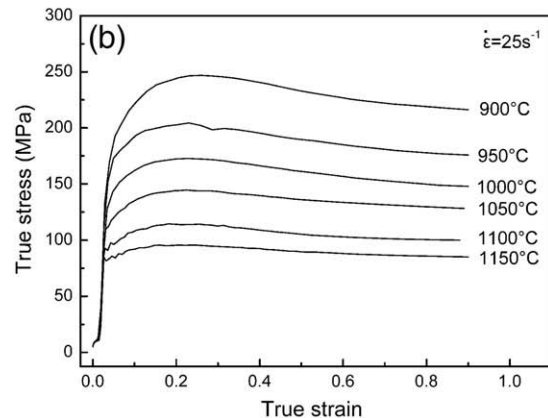
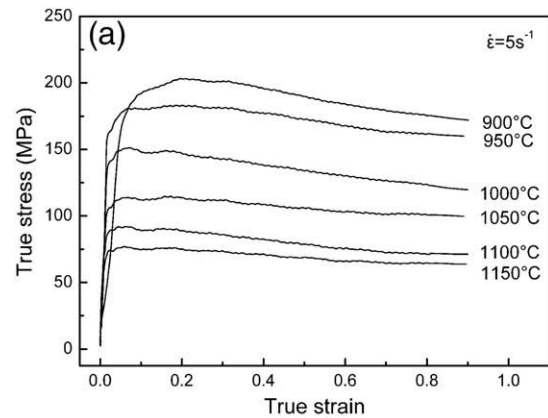
#### 3.1. Flow Stress

Fig. 2 shows the phase diagram calculated by using the Thermo-calc software. It can be seen that only ferrite and austenite were formed at the present experimental temperatures. Ferrite increases with increasing the deformation temperature while austenite decreases instead.

Fig. 3 shows true stress–true strain curves obtained at different temperatures and medium–high strain rates. It can be noted that flow stress increases when strain rate increases and temperature decreases. All the flow curves demonstrate similar characteristics. The flow stress increases to a peak value with the increase in strain and then decreases slowly as the strain further increases. The critical strain to the peak stress increases with the decrease in temperature and with the increment of strain rate. Furthermore, at strain rate of  $50 \text{ s}^{-1}$ , the flow curves reveal obvious strain hardening features and exhibit significant waviness at strain lower than 0.4, which may be attributed to the fact that the severely uneven distribution of strain in the ferrite and austenite phases at very high strain rates in the early stage of deformation process. The discontinuous or localized softening of the ferrite occurs because the strain in ferrite is hindered by the harder austenite and more strain obtained in austenite accelerates its occurring of dynamic re-crystallization.

#### 3.2. Characterizations of Activation Energy and Z Parameter

Peak stress values were obtained in formerly illustrated curves under different working conditions. Eq. (1) was employed to describe the peak stress as a function of deformation



**Fig. 3** – Flow curves of 00Cr23Ni4N duplex stainless steel at different hot working conditions: (a)  $5 \text{ s}^{-1}$ ; (b)  $25 \text{ s}^{-1}$ ; and (c)  $50 \text{ s}^{-1}$ .

temperature and strain rate for deformation conditions in application. After taking logarithm, it can be written as:

$$\ln[\sinh(\alpha \cdot \sigma_p)] = \frac{1}{n} \ln \dot{\epsilon} + \frac{Q}{nRT} - \frac{1}{n} \ln A. \quad (4)$$

Linear statistical regression analyses can determine the values of  $A$ ,  $n$  and  $Q$ . Before regression, the value of constant  $\alpha$  is firstly estimated to be  $0.012 \text{ MPa}^{-1}$  [9,10]. Figs. 4 and 5 exhibit the relationships of  $\ln[\sinh(\alpha \cdot \sigma_p)]$  vs  $\ln \dot{\epsilon}$  and  $\ln[\sinh(\alpha \cdot \sigma_p)]$  vs  $10000/T$ , in which the values of  $A$ ,  $n$  and  $Q$  determined by this analysis are  $A = 2.7 \times 10^{10} \text{ s}^{-1}$ ,  $n = 2.6$  and  $Q = 263.4 \text{ kJ/mol}$ , respectively. Previous studies have shown that the activation

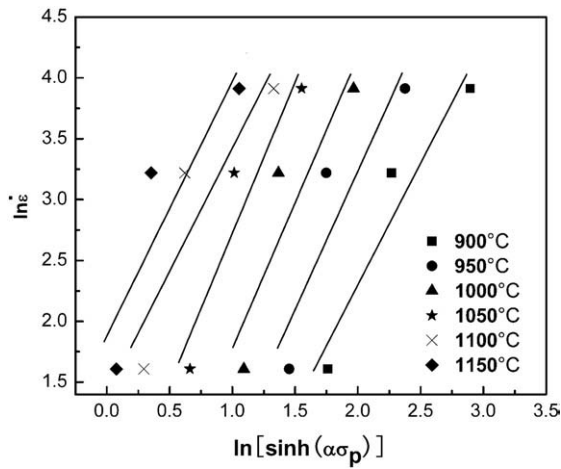


Fig. 4 – Variations of peak stress with strain rate for 00Cr23Ni4N duplex stainless steel at different temperatures.

energy of deformation for duplex stainless steel is of great differences in terms of different processing parameters, i.e. strain rate, temperature and strain. Temperature is considered as a critical and influential factor owing to the distinct dual phase scale with enhancing temperature. Higher than about 1050 °C, the ferrite in the steel crosses 50% threshold and becomes the majority phase (Fig. 2). Hence, the activation energy under different temperature ranges is also confirmed in the present work. The activation energy calculated at high temperatures (1050–1150 °C) is lower than that at low temperatures (900–1050 °C), amount to 212.1 kJ/mol and 301.5 kJ/mol, respectively. Indeed, the Q value can be used to reflect the dominant mechanism during hot working, such as dynamic re-crystallization and dynamic recovery. It is well known that the Q value, for dynamic re-crystallization in austenite is higher than that of dynamic recovery in ferrite. Therefore, the declination of Q value with temperature is attributable to the fact that a lower volume fraction of austenite and a higher content of ferrite form in high temperatures, during which ferrite softening will be the dominant mechanism [7].

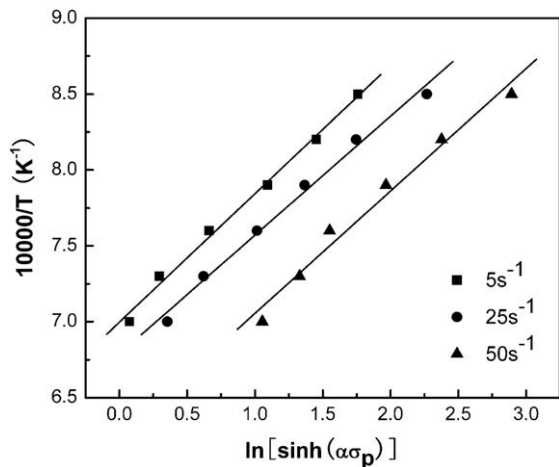


Fig. 5 – Variations of peak stress with temperature for 00Cr23Ni4N duplex stainless steel at different strain rates.

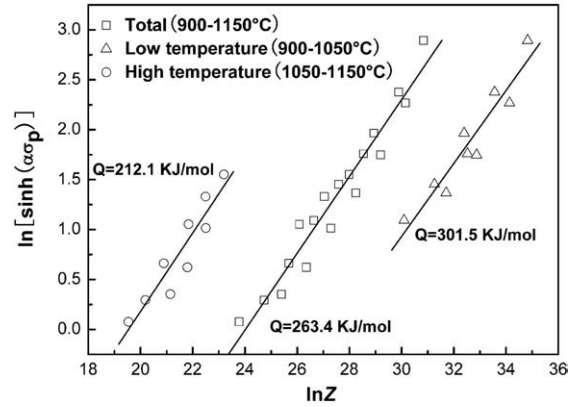


Fig. 6 – Variations of peak stress with Z parameter for 00Cr23Ni4N duplex stainless steel at different deformation conditions.

According to Eq. (1) and the obtained parameter values, the Z parameter can be written as:

$$Z = \dot{\epsilon} \exp(263,400 / RT) \tag{5}$$

Z values under the experimental conditions are calculated by using Eq. (5). The relationship of the Z parameter and peak stress is shown in Fig. 6. It is clear that the data calculated are very well fit linearly to experiments. The peak stress indeed increases with increasing the Z parameter. Lower Z values are obtained at higher deformation temperatures, the corresponding Q value is low.

### 3.3. Processing Map and Microstructure

Fig. 7 shows the processing map obtained at the strain of 0.8, which based on the flow stress data at different temperatures and strain rates demonstrated above. Contour numbers represent efficiency of power dissipation and shaded region corresponds to instability. High efficiency of power dissipation indicates the material dissipates more energy for microstructural changes, and then is benefit to hot deformation. It is clearly seen that the map exhibits two domains (A and B) with peak power dissipation efficiency of about 40% and 65% respectively (the upper panel). However, the region on the under panel presents low efficiency values, which illustrates high strain rate may make more contributions to the deformation. The flow instability regions can be observed at 950 °C and low strain rate (5 s<sup>-1</sup>), where the efficiency value is also negative.

Typical microstructures obtained on the specimen after deformed are shown in Fig. 8. As can be seen in Fig. 8a, corresponding to the microstructure in domain A (1000 °C, 50 s<sup>-1</sup>), the substructure formed by dynamic recovery in ferrite and mixed austenite grain structure, consisting of partial re-crystallized grains and original grains elongated along the vertical direction of the deformation have obtained. By increasing temperature at high strain rates, austenite with small islands indeed decreases and its dynamic re-crystallization process becomes more sufficient. Furthermore, the dynamic re-crystallization of ferrite is easily observed under this condition,

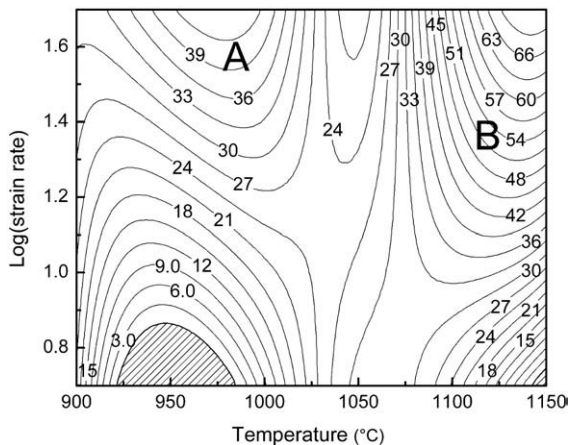


Fig. 7 – The processing map of 00Cr23Ni4N duplex stainless steel at the strain of 0.8.

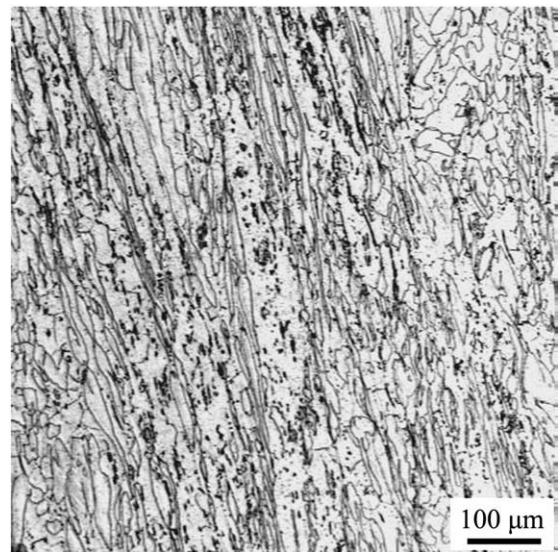


Fig. 9 – The microstructure for the specimen after deformed at the unstable region (950 °C, 5 s<sup>-1</sup>).

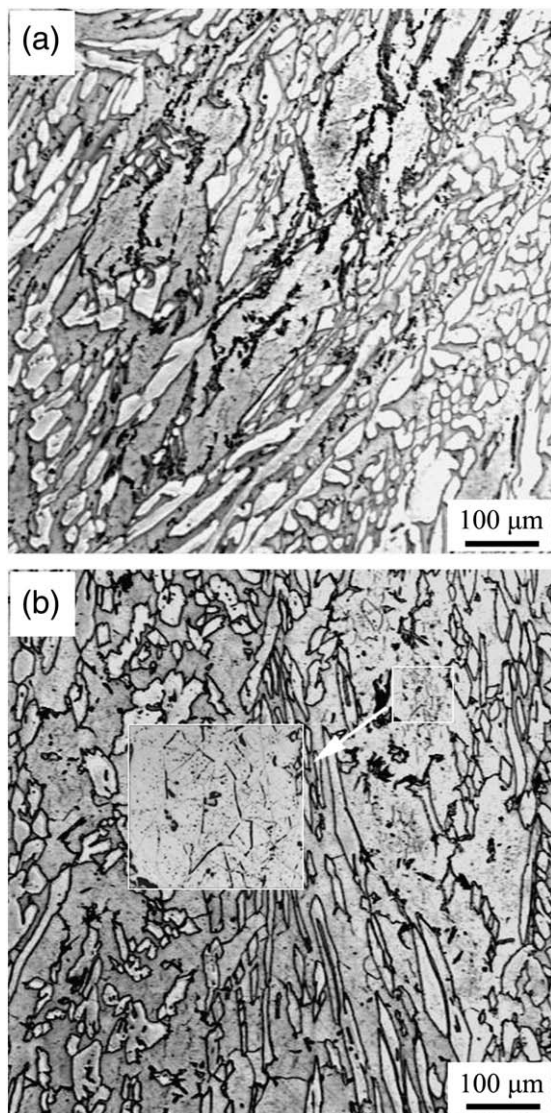


Fig. 8 – Microstructures for the specimens after deformed in the region with peak efficiency of power dissipation: (a) 1000 °C, 50 s<sup>-1</sup>; and (b) 1150 °C, 50 s<sup>-1</sup>.

as shown in Fig. 8b, which may result in the enhanced power dissipation efficiency during hot deformation. It is known that the dynamic restoration behavior of duplex stainless steel is correlated with the softening mechanism of constituent phases. As commonly ferrite softens by dynamic recovery, called soft phase, and austenite softens by dynamic re-crystallization, called hard phase. Coexistence of hard austenite and soft ferrite at high temperatures is found to result in a strain mostly accommodating by the ferrite phase at the early stages of deformation. At higher strains, load is transferred from ferrite to austenite leading to increment of dislocation density in the latter till triggering of dynamic re-crystallization. So from Fig. 3 the shapes of all the true stress–strain curves are typical for the occurrence of dynamic re-crystallization with extending of strain. The austenite in duplex stainless steel may also obtain more strain with increasing strain rate at low temperatures, which may accelerate its dynamic re-crystallization behavior. Meanwhile, after the application of very high strain rates and sufficiently high temperatures, the local presence of dynamic re-crystallization in ferrite is promoted [21], which results in a lower Z value and a higher efficiency of power dissipation in the corresponding conditions.

No wedge and macro-crack are found in the specimen deformed at flow instability region, at least under the present condition (950 °C, 5 s<sup>-1</sup>) and the microstructure is shown in Fig. 9. No dynamic re-crystallization has occurred in both phases and visible flow location of austenite in the smooth matrix of ferrite might have caused the instability during hot deformation.

In an industrial practice, highest possible strain rates and lowest possible stresses are preferred from productivity viewpoint [18]. Considering this reason, it can be concluded that the range of strain rates from 10 to 30 s<sup>-1</sup> and temperatures from 1075 to 1150 °C is an optimum zone for hot deformation of 00Cr23Ni4N duplex stainless steel.

#### 4. Conclusions

The hot deformation behavior of 00Cr23Ni4N duplex stainless steel under medium–high strain rates is studied in compression at temperatures from 900 to 1150 °C. Below are the results obtained:

- (1) The classical hyperbolic sine equation can be adopted to describe the relationship among the peak stress, strain rate and deformation temperature, in which the mean activation energy,  $Q$  and  $n$  are 263.4 kJ/mol and 2.6 respectively.
- (2) The lower the  $Z$  parameter, the lower the flow stress, the lower the activation energy and the more easily the dynamic re-crystallization may occur.
- (3) Based on the processing map, high strain rate facilitates the power dissipation by microstructure evolution during hot working process. The domain with peak efficiency of power dissipation is in the temperature range of 1075–1150 °C and the strain rate range of 10–50 s<sup>-1</sup>, in which both ferrite and austenite dynamic recrystallizations can be obtained. Meanwhile, the unstable domains through flow localization can be observed at 950 °C and 5 s<sup>-1</sup>.
- (4) The condition with high strain rate and sufficiently high temperature is beneficial to hot deformation procedure for 00Cr23Ni4N duplex stainless steel. It can be concluded that the range of strain rates from 10 to 30 s<sup>-1</sup> and temperatures from 1075 to 1150 °C is an optimum zone for hot deformation of 00Cr23Ni4N duplex stainless steel in an industrial practice.

#### Acknowledgements

This work is supported by the project of Shaanxi Province science and technology research and development program (2010K10-13).

#### REFERENCES

- [1] Jimenez JA, Carsi M, Ruano OA. Characterization of a  $\delta/\gamma$  duplex stainless steel. *J Mater Sci* 2000;35:907–15.
- [2] Koztowski RH. Composite of austenitic–ferritic stainless steel. *J Mater Process Tech* 1995;53:239–46.
- [3] Lin G, Zhang ZX, Song HW, Tong JR, Zhou CD. Investigation of the hot plasticity of duplex stainless steel. *J Iron Steel Res Int* 2008;15(6):83–6.
- [4] Badji R, Bouabdallah M, Bacroix B, Kahloun C, Belkessa B, Maza H. Phase transformation and mechanical behavior in annealed 2205 duplex stainless steel welds. *Mater Charact* 2008;59:447–53.
- [5] Cabrera JM, Mateo A, Llanes L, Prado JM, Anglada M. Hot deformation of duplex stainless steels. *J Mater Process Tech* 2003;143–144:321–5.
- [6] Fan GW, Liu J, Han PD, Qiao GJ. Hot ductility and microstructure in casted 2205 duplex stainless steels. *Mater Sci Eng A* 2009;515:108–12.
- [7] Farnoush H, Momeni A, Dehghani K, Aghazadeh Mohandesi J, Keshmiri H. Hot deformation characteristics of 2205 duplex stainless steel based on the behavior of constituent phases. *Mater Des* 2010;31:220–6.
- [8] Iza-Mendia A, Pinol-Juez A, Urcola JJ, Gutierrez I. Microstructural and mechanical behavior of a duplex stainless steel under hot working conditions. *Metall Mater Trans A* 1998;29:2975–86.
- [9] Evangelista E, McQueen HJ, Niewczas M, Cabibbo M. Hot workability of 2304 and 2205 duplex stainless steel. *Can Metall Quart* 2004;43(3):339–54.
- [10] Liu JT, Chang HB, Wu RH, Hsu TY, Ruan XY. Investigation on hot deformation behavior of AISI T1 high-speed steel. *Mater Charact* 2000;45:175–86.
- [11] Tan SP, Wang ZH, Cheng SC, Liu ZD, Han JC, Fu WT. Processing maps and hot workability of Super304H austenitic heat-resistant stainless steel. *Mater Sci Eng A* 2009;517:312–5.
- [12] Prasad YVRK, Sasidhara S. *Hot Working Guide: A Compendium of Processing Maps*. America: ASM; 1997.
- [13] Srinivasan N, Prasad YVRK, Rama Rao P. Hot deformation behaviour of Mg–3Al alloy — a study using processing map. *Mater Sci Eng A* 2008;476:146–56.
- [14] Meng G, Li BL, Li HM, Huang H, Nie ZR. Hot deformation and processing maps of an Al–5.7 wt.% Mg alloy with erbium. *Mater Sci Eng A* 2009;517:132–7.
- [15] Prasad YVRK, Seshacharyulu T. Processing maps for hot working of titanium alloys. *Mater Sci Eng A* 1998;243:82–8.
- [16] Wu K, Liu GQ, Hu BF, Li F, Zhang YW, Tao Y, et al. Characterization of hot deformation behavior of a new Ni–Cr–Co based P/M superalloy. *Mater Charact* 2010;61:330–40.
- [17] Fang YL, Liu ZY, Song HM, Jiang LZ. Hot deformation behavior of a new austenite–ferrite duplex stainless steel containing high content of nitrogen. *Mater Sci Eng A* 2009;526:128–33.
- [18] Narayana Murty SVS, Nageswara Rao B, Kashyap BP. Identification of flow instabilities in the processing maps of AISI 304 stainless steel. *J Mater Process Tech* 2005;166:268–78.
- [19] Wang ZH, Fu WT, Wang BZ, Zhang WH, Lv ZQ, Jiang P. Study on hot deformation characteristics of 12%Cr ultra-super-critical rotor steel using processing maps and Zener–Hollomon parameter. *Mater Charact* 2010;61:25–30.
- [20] Wu J. *Duplex Stainless Steel*. China: Metallurgical Industry Press; 1999.
- [21] Kato K, Saito Y, Sakai T. Investigation of recovery and recrystallization during hot rolling of stainless steels with high speed laboratory mill. *Trans ISIJ* 1984;24:1050–4.